Sparse matching via point and line feature fusion for robust aerial triangulation of photovoltaic power stations’ thermal infrared imagery

Tao Ke [1,2], Zhouyuan Ye [1], Xiao Zhang [3], Yifan Liao [1], Pengjie Tao [1,2,*]

[1] School of Remote Sensing and Information Engineering, Wuhan University, Wuhan 430079, China - ketao@whu.edu.cn, Lionel16@whu.edu.cn, liaoyifan01@whu.edu.cn, pjtao@whu.edu.cn
[2] Hubei Luojia Laboratory, Wuhan 430079, China
[3] CCCC Second Highway Consultants Co. Ltd, Wuhan 430056, China - xiaozhxr@163.com

Keywords: Image Matching, Photovoltaic Panel, Thermal Infrared Image, Repetitive Texture, Line Feature.

Abstract

In this paper, we present a novel matching method tailored for unmanned aerial vehicle (UAV) thermal infrared images of photovoltaic (PV) panels characterized by highly repetitive textures. This method capitalizes on the integration of point and line features within the image to obtain reliable corresponding points. Furthermore, it employs multiple constraints to eliminate mismatched features and get rid of the interference of repetitive textures on feature matching. To verify the effectiveness of the proposed method, we used an UAV equipped with the DJI Zenmuse H20T thermal infrared gimbal to capture 3767 images of a PV power station in Guangzhou, China. Experiments demonstrate that, for UAV thermal infrared images of PV panels, our method outperforms the state-of-the-art techniques in terms of the density of matching points, matching success rate and matching reliability, consequently leading to robust aerial triangulation results.

1. Introduction

Due to energy shortages and environmental pollution, solar energy, as a renewable and clean energy source, is increasingly receiving widespread attention from people. People's utilization of solar energy is mainly achieved through photovoltaic (PV) power stations, and as an important component of PV power stations, the operation of PV panels directly affects the efficiency and stability of power generation, and may even cause safety issues, leading to significant property losses. In addition, the vast majority of large-scale PV power stations in China are built in suburban areas or desert wastelands, which are geographically remote, have complex environments, and are sparsely populated, thereby increasing the likelihood of PV panel failures and the difficulty of maintenance. Therefore, accurate and efficient monitoring of the working status of the PV panels is of great significance for PV power stations.

The traditional monitoring methods for the working status of PV panels mainly include electrical characteristics method (Jia, 2021), electroluminescence method (Bu, et al, 2022), laser detection method and visual inspection method (Wang, et al, 2021), and so on. Due to the fact that PV power stations are often built in suburban areas, harsh environments, and sparsely populated areas, traditional monitoring methods often consume a lot of manpower, material resources, and time.

In recent years, with the development of artificial intelligence technology and the improvement of remote sensing image resolution, some new methods based on remote sensing images have been proposed. For example, Liu et al. (2023) studied the use of deep learning methods, they successfully segmented and extracted PV panels from high-resolution remote sensing images. Zhao et al. (2023) and Li et al. (2023) used different methods and means, solved the problem of detecting defects in PV panels from images. Kaplani (2012) also studied the issue of using infrared images to detect the presence of thermal spots in PV arrays. It can be seen that with the development of technology, people have begun to use unmanned aerial vehicles (UAVs) equipped with thermal infrared imaging devices to monitor PV panels. These methods can not only improve the efficiency, but also reduce the workload of relevant personnel and the cost of monitoring.

Considering factors such as resolution, image size, and ease of image acquisition, compared to other photogrammetric methods such as aerial photography and satellite photography, UAV photography has more advantages in observing PV panels.

In order to monitor the working status of PV panels using a thermal infrared imager mounted on UAV, it is necessary to perform aerial triangulation and surface reconstruction on the thermal infrared images. In this process, obtain sparse tie points between image though feature matching is a very important step. Most commonly used feature matching algorithms include SIFT (Lowe, 2004), SURF (Bay, et al, 2006), and so on.

However, there are highly repetitive textures in the UAV thermal infrared PV panel images, which bring great challenges to the image matching. For example, Figure 1 shows two adjacent thermal infrared PV panel images, whose textures, grayscales, gradients, structures are highly similar, making it difficult for even naked eye to determine corresponding points.

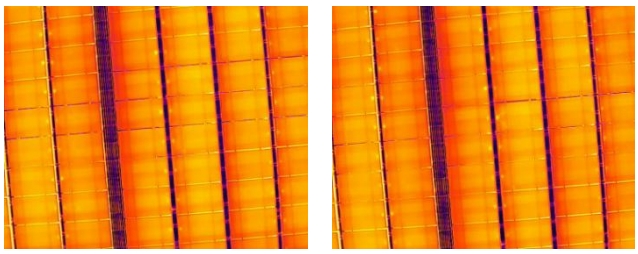

(*a*) Left image (*b*) Right image
Figure 1. Two UAV thermal infrared PV panel images with highly repetitive textures and high similarity

To address the issue of repetitive textures in PV panel images, we adopt a matching method that combines point and line

* Corresponding author

features under multiple criteria. Compared to the methods which only using point features, line features are also adopted to match corresponding points, which can not only increase the number of image features, but also provide more constraint conditions. Through these constraint conditions, we can create more criteria to eliminate mismatched features after initial matching. Furthermore, the accuracy of matching has been improved.

2. Methodology

The specific process of the proposed sparse matching method is shown in Figure 2.

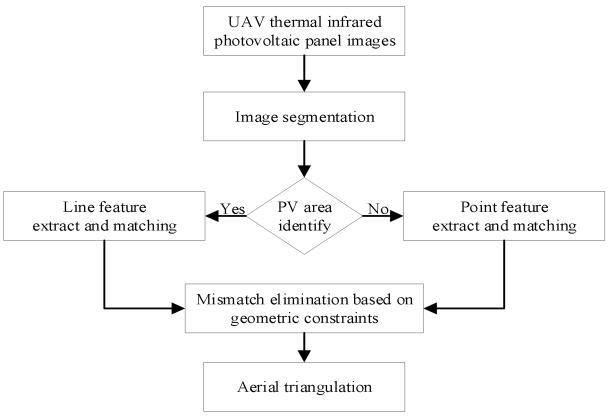

Figure 2. Workflow of the proposed sparse matching method based on the combination of point and line features

First of all, we divide each image into several blocks. Then, we identify the PV panel area for each block. If a block belongs to the PV panel area, we perform line feature extraction and matching on it. Otherwise, point feature extraction and matching will be used as a supplementary method. After that, according to geometric constraints of point features or line features, we will create some criteria to eliminate the mismatched points in the initial matching results. Finally, we use filtered image features for aerial triangulation.

2.1 Recognition of PV areas in images

As we all know, in thermal infrared images, the color tone of a ground object is highly correlated with its surface temperature: the higher the surface temperature of the object, the brighter its color tone after imaging, presenting a bright yellow to red color; On the contrary, if the surface temperature of the object is lower, its color tone will be darker after imaging, presenting a blue purple to dark purple color.

Due to sunlight exposure, the surface area of PV panels accumulates a large amount of heat, resulting in temperatures generally exceeding 60°C (Wu, et al, 2024 & Du, et al, 2016) and even reaching up to 90°C (Kurtz, et al, 2009). The installation of PV panels is generally located at the top of a building, and the background in the UAV thermal infrared PV panel image is likely to be roads, vegetation, and houses, with a surface temperature much lower than that of the PV panels. After imaging, there is a significant difference in color tone between the background area (i.e. non-PV panel area) and the PV panel area, as shown in Figure 3(*a*). Therefore, based on the tone threshold method, the PV panel area in the image can be distinguished from the background area.

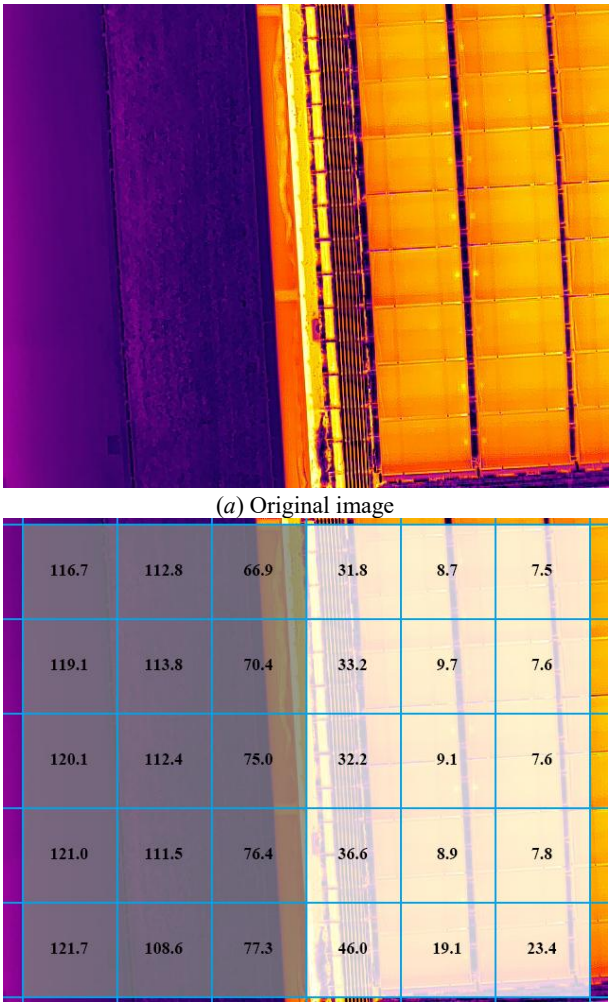

(*a*) Original image

(*b*) Result image

Figure 3. PV panel area (left) and non-PV panel area (right) in an original thermal infrared image and its result image

It is not difficult to find that in the RGB color system, the R and G components of the RGB values corresponding to the red and yellow colors are very high and close to 255, while the B component is very low and close to 0. The B component of the RGB values corresponding to the blue and purple colors is very high and usually greater than 128, even close to 255; the G component is very low and close to 0; and the R component has weak regularity.

Therefore, we first divide the images into small blocks, for example, 100 × 100 pixels for each block. Then, we count the RGB mean of each block respectively, and use its B component as the classification standard, 64 as the threshold, to divide the PV panel area based on this. If the B component of the RGB mean is greater than 64, then this block is considered as a non-PV panel area. Otherwise, it is considered as a PV panel area. After recognition of PV areas, the result is shown in Figure 3(*b*). Where, the grey blocks are non-PV areas, and the white blocks are PV areas. The number in each block is the average value of the B component of that block.

For the PV panel areas, in order to more accurately extract line features for subsequent matching, the Canny operator (Canny, 1986) is first used for edge detection, as shown in Figure 4. Then, line feature extraction and matching are performed.

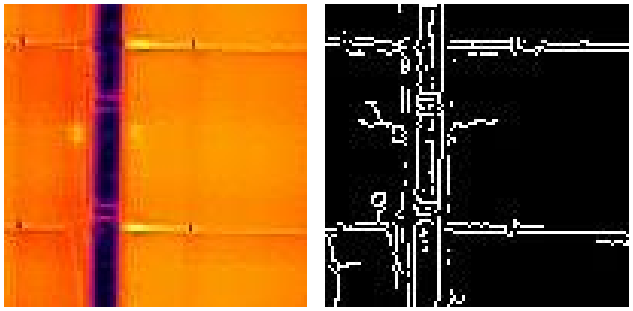

(*a*) Original image (*b*) Edge detection image
Figure 4. Image edge detection with Canny operator

For the non-PV panel areas, due to unclear or insufficient line features on the image, we use SIFT algorithm to extract and match point features as a supplementary method.

2.2 Image matching based on line features

For areas containing PV panels, as each panel is a regular rectangle of similar size and arranged neatly, there are a large number of line features. Image matching based on line features was developed to obtain tie points between images. A line segment detector (LSD) (Rafael, et al, 2010) algorithm can be used to extract these line features, and based on this, line band descriptor (LBD) (Zhang, et al, 2013) algorithm can be used for line feature matching.

The matched homonymous line features have highly consistent and stable geometric features. Therefore, the following criterions can be used to eliminate gross errors and improve the accuracy of feature matching.

2.2.1 Length criterion

The length criterion refers to calculate the lengths D_1 and D_2 of a set of line segments corresponding to the matching results of two images. If the ratio of the longer to shorter length of the group of line segments is greater than the threshold Δ_1, it will be considered that the length of this group of line segments is inconsistent. Line segments with inconsistent lengths cannot be corresponding line segments, so the matching of this group of line segments is incorrect and should be removed.

Due to the stable flight altitude of the UAV and the consistent height of all PV panels, as well as the similar height of all non-PV panel areas, and the relatively small image size of a single image, the impact of image distortion can also be ignored. Therefore, the length between the corresponding line segments on the image can be directly used as the judgment basis, without the need to project the line segments on the image to calculate their actual ground coordinates, for reducing the computational complexity of the algorithm.

2.2.2 Slope criterion

The slope criterion refers to calculate the absolute values k_1 and k_2 of the slopes of a set of line segments corresponding to the matching results of two images separately. If the absolute value of the slope difference of the group of line segments is greater than the threshold Δ_2, it will be considered that the slope of this group of line segments is inconsistent. Line segments with inconsistent slopes cannot be of the corresponding line segments, so the matching of this group of line segments is incorrect and should be removed.

Due to the fact that the vast majority of images (excluding several images at the beginning and end of each airstrip) can be considered as a combination of translational and 180 degrees rotational transformations, there exists a specific relationship between the slopes of the corresponding line segments, that is, the slopes are equal or opposite to each other. That is to say, the absolute values of the slopes are equal.

To determine whether two images are at the beginning and end of a single strip, it is possible to directly use the *yaw* value in the elements of exterior orientation for reading. The *yaw* value of the image in the middle of the strip is basically stable, while the *yaw* value of the image at the beginning and end of the strip will undergo rapid and significant changes due to the UAV's turning flight, making it easier to identify.

The proportion of images with large angle rotation at the beginning and end of each strip is relatively small, and there are not many line features, which can be skipped directly without judging based on the slope criterion.

2.2.3 Coordinate difference criterion

The coordinate difference criterion refers to calculating the difference between the image coordinate values of all the corresponding line segments on two images, and conducting adjustment calculations to detect the gross errors in the image point coordinate values, treating them as data with significant deviations from the difference in the image point coordinate values between normal two points. A line segment with a significant deviation in the difference between the measured values of the point coordinates cannot be the corresponding line segment. Therefore, the matching of this group of line segments is incorrect and should be removed.

The principle is that for images within the same strip or images between odd numbered strips (excluding several images at the beginning and end of each aerial strip), especially for two adjacent images in the photography order, it can be considered that there is only a translation transformation. Therefore, the difference in the measured values of the image coordinates between the corresponding line segments on it should be stable, at least with little variation. After the screening of the two criteria described in sections 2.2.1 and 2.2.2, the coordinate difference between several corresponding line segments on the same horizontal plane has been basically stable. However, some PV panels have inclination angles, and there may still be matching errors.

In order to continue filtering out these matching errors, the filtering results mentioned earlier can be used as the benchmark for bundle adjustment. After bundle adjustment, the corresponding line segments with coordinate differences greater than three times the root mean square error (RMSE) can be selected and eliminated.

As mentioned in section 2.2.2, it is still possible to directly use the *yaw* value in the elements of exterior orientation to determine whether the image is in the same strip (or an odd number of aerial apart) and whether it is a number of images with large angle rotations at the beginning and end of the strip. This will not be elaborated here.

2.3 Image matching based on point features

For other areas without PV panels or with only a small amount of PV panels, due to the unclear line features, after

experimental comparison and verification, although the extracted line features are not less than the images of areas with a large number of PV panels, the correctly matched line features are very few, making it difficult to meet the quantity requirements for aerial triangulation. Therefore, the SIFT algorithm is used as a supplement.

2.3.1 Coverage range criterion

For the matched point features, first, use the "coverage range criterion" of the images for evaluation. Its theoretical basis is the inversion formula of the Collinearity Equation.

Considering the photography method of UAV images, the obtained image is approximately an orthophoto, and the image spatial coordinates of the object space points on the image are consistent with the image spatial auxiliary coordinates, that is:

$$X = x, Y = y, Z = -f \tag{1}$$

Where, assuming there is a ground point A, $(x, y, -f)$ and (X, Y, Z) are the image space coordinates and image space auxiliary coordinates of A's image point respectively.

In addition, fully considering that the maximum ground range covered by the image should not be based on the elevation of the features, but on the ground of the four corner points. Therefore, the average ground elevation $H_{average}$ of the measurement area should be used instead of the ground elevation Z_A of corner point A. Substituting it together with $Z = -f$ in Equation (1), the scale factor λ in Collinearity Equation is as follows:

$$\lambda = \frac{H_{average} - Z_S}{-f} \tag{2}$$

Where, S is photography center, its coordinate in the object space coordinate system is (X_S, Y_S, Z_S); and the coordinate in the object space coordinate system of ground point A is (X_A, Y_A, Z_A).

By substituting the measured coordinates of the four corner points of an image, which are $(0,0)$, $(0, y_{max})$, $(x_{max}, 0)$ and (x_{max}, y_{max}), and Equation (2) into Collinearity Equation, the object space coordinates of the four corner points of the image can be calculated, and then the ground range covered by the image can be obtained through simple mathematical calculations.

If there are matching points between two images in the pre-matching process, calculate the overlapping degree of the ground coverage range corresponding to these two images to the area of the ground coverage range corresponding to each image. As shown in Figure 5, there are 3 cases of relative position relationship.

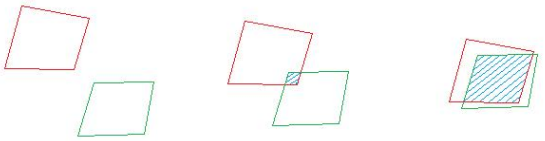

(*a*) No overlap (*b*) Low overlap (*c*) High overlap
Figure 5. Three cases of the relative position of two images

If the overlapping degree of the image does not reach the threshold Δ_3, including the case where the two images do not overlap at all, it is considered as not meeting the requirements of image matching. The matching results of these two images will be removed.

2.3.2 Reprojection error criterion

Secondly, use the "reprojection error criterion" for evaluation. It is achieved by calculating the projection difference between the reprojection after forward intersection and the original image point.

After going through the previous step, we assume that all remaining matching points in the images are correct. So, as shown in Figure 6, we can perform forward intersection on matching points, there will be two situations.

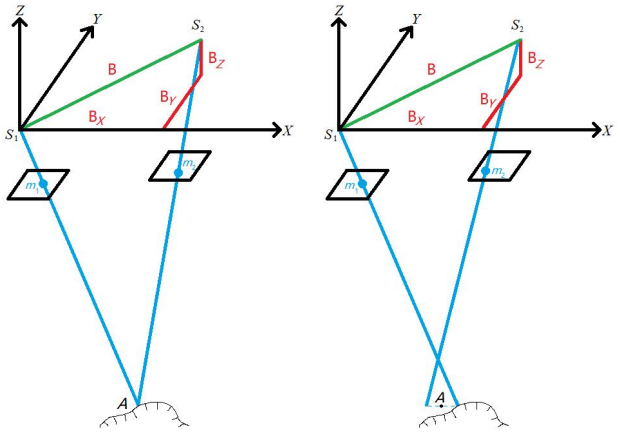

(*a*) Correct matching points (*b*) Wrong matching points
Figure 6. Forward intersection of matching points

For each correctly matched set of corresponding points, if the influence of various errors is ignored, the two photography rays S_1m_1 and S_2m_2 are coplanar and intersect at the ground point A, as shown in Figure 6(a). Where, m_1 and m_2 are the matching points on the left image and right image respectively, S_1 and S_2 are the photography center points of the left image and right image respectively.

In this case, using the Collinearity Equation, perform another projection on the ground point $A(X_A, Y_A, Z_A)$. We call it "reprojection". Taking the right image as an example for reprojection, the coordinate of m', which is the image point obtained after reprojection, is (x', y'). Considering the influence of various measurement errors, $m'(x', y')$ should be near $m_2(x_2, y_2)$.

On the contrary, for each incorrectly matched set of corresponding points, S_1m_1 and S_2m_2 are skew lines, which is impossible to intersect in real space, as shown in Figure 6(b). In this case, the calculated ground point $A(X_A, Y_A, Z_A)$ is an imaginary point. If we continue to perform projection on the imaginary ground point A, the obtained image point m' is highly likely to be far from m_2.

So, a threshold Δ_4 should be set here. If the projection difference (i.e. distance between m' and m_2) is greater than the threshold Δ_4, it will be considered that m_1 and m_2 are not the corresponding points and the matching results should be removed.

3. Experiment

3.1 Dataset

In order to verify the reliability of the proposed method and the accuracy of aerial triangulation based on it, a series of comparative experiments were conducted. The measurement area of the UAV thermal infrared PV panel image used in the experiment is located at the Baiyun District, Guangzhou, Guangdong Province, China.

In terms of images, 3767 thermal infrared PV panel images were captured by UAV. The main measured objects in each area are several neatly arranged PV panel arrays. And main parameters of the images captured by DJI Zenmuse H20T camera are as follows: The size of the image is 640 × 512 pixels; the field of view is 40.6°; the pixel size is 12.2873 μm; and the focal length is 13.5 mm.

The schematic diagram of the survey area is shown in Figure 7.

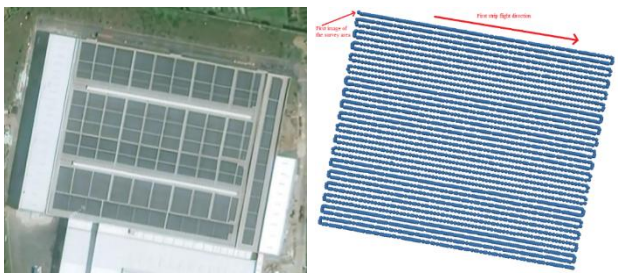

(*a*) Overview of the test area (*b*) UAV flight trajectory

Figure 7. Overview of the test area and the UAV flight path

3.2 Baselines and implementation details

The proposed method was compared with SIFT, Agisoft Metashape, and COLMAP (Schoenberger, 2016), to verify its effectiveness. The relevant parameters set in the Agisoft Metashape and COLMAP software used are as follows:

Agisoft Metashape Professional 2.0.2.16102 (64bit): matching accuracy is highest; generic preselection; reference preselection is source; key point limit per million pixels are 100000; tie point limit is 100000.

COLMAP 3.7-windows- no-cuda: camera model is OPENCV; shared per sub-folder; parameters from EXIF; maching method is Spatial; is_gps; ignore_z; max_num_neighbors are 350; max_distance is 100.

All values of thresholds mentioned above are shown in Table 1.

Parameters	Value
Δ_1	0.1
Δ_2	0.2
Δ_3	50%
Δ_4	3 pixels

Table 1. Values of thresholds

For fair comparison, Agisoft Metashape was used to perform bundle adjustment using tie points obtain from different image matching methods and evaluate the processing results. For the matched tie points from the proposed method, SIFT method and COLMAP, they were first organized as the XML format, and then imported into Agisoft Metashape for bundle adjustment.

3.3 Results

The statistical data results of the proposed method and the baseline methods are shown in Table 2. It can be seen from Table 2 that the proposed method extracts and matches a large number of image feature points (including point features and the starting points and ending points of line features), and the number of feature points used in aerial triangulation is the highest (100% utilization rate). After aerial triangulation, all images were successfully aligned, and the root of mean square adjusted values of positions of images in the XYZ directions were the smallest. This indicates that compared to baseline methods, the proposed method has the highest matching success rate and the best results from aerial triangulation.

Method	Aligned Images	Total Points	Used Points	Root of Mean Squared Adjusted Values of positions of images (cm)		
				X	Y	Z
The proposed method	3767	2,465,068	2,465,068	26.0	23.4	59.4
SIFT	3685	1,839,516	1,834,869	85.4	67.4	214.6
Agisoft Metashape	3762	1,766,141	1,086,293	221.9	71.4	196.0
COLMAP	2185	5,604,115	140,392	Aerial triangulation failed, no valid data		

Table 2. Comparison of the experimental results of the proposed method and the baseline methods

As for SIFT method, the total number of points extracted and matched is relatively small, although its utilization rate is also high (over 99%). The insufficient number of matching points has led to a decrease in the number of aligned images. Not 100% utilization rate indicates that there are still errors in the matching points, resulting in an increase the root of mean square adjusted values of positions of images in the XYZ directions.

As for Agisoft Metashape's method, although total number of points are similar to SIFT method, its utilization rate is lower, which indicating more errors in the matching points, and resulting in a higher root of mean square adjusted values of positions of images in the XYZ directions.

Furthermore, to incorporate as many images as possible into the image network, the Agisoft Metashape has many extremely unnatural, discontinuous, and non-smooth undulations in its strip. This will be further discussed in the following text.

As for COLMAP's method, it extracts and matches the largest number of image feature points, but the utilization rate is less than 3%. Massive mismatched points cause aerial triangulation to fail. This proves that blindly increasing the number of matching points without considering accuracy cannot solve such problems.

The adjusted tie point clouds of four methods are shown in Figure 8. From Figure 8(*a*), it can be observed that the adjusted tie points of the proposed method are complete, with uniform

and dense point features, covering all PV panel areas. There are only empty holes in non-key areas such as the road on the north side, greenbelts on the east and southwest sides (these features correspond to few image features and are also distributed at the edges of the measurement area, which has little impact on aerial triangulation), indicating that the proposed method has successfully matched the correct corresponding points in all images with a certain degree of overlap. From Figure 8(*b*) and 8(*c*), there are lots of empty holes in the PV panel area. That indicates that there are errors or omissions in the matching points. From Figure 8(*d*), the adjusted tie points cloud can even be chaotic. That explains why its aerial triangulation failed.

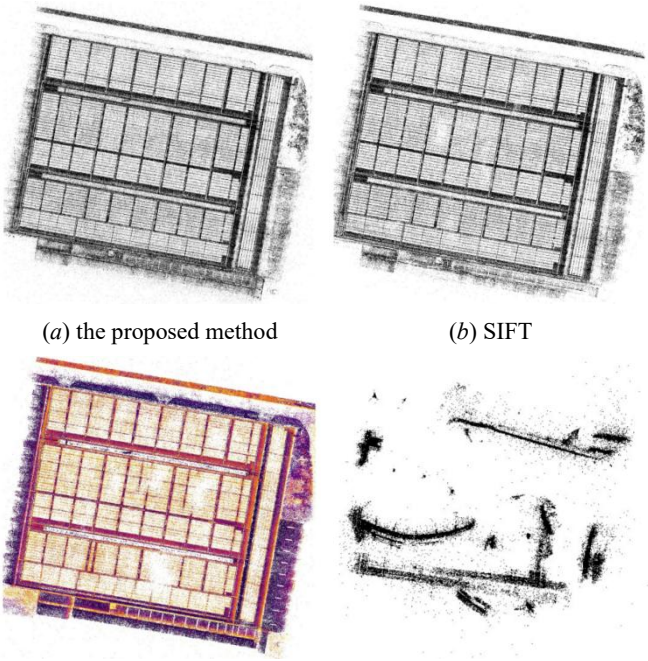

(*a*) the proposed method (*b*) SIFT

(*c*) Agisoft Metashape (*d*) COLMAP

Figure 8. The distributions of the adjusted tie points from the proposed method and baseline methods

In addition, in order to align as many images as possible, Agisoft Metashape’s method has many extremely unnatural, discontinuous, and non-smooth undulations in its strip. The sparser part and empty holes of the adjusted tie points shown in Figure 8(c) is actually due to errors in the position of the fitted image after aerial triangulation, resulting in voids between several images in the same strip as shown in Figure 9.

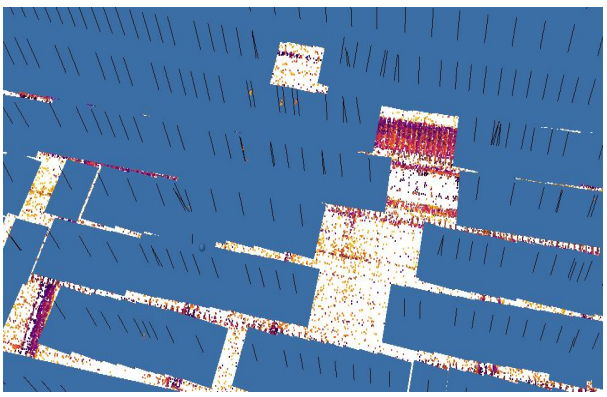

Figure 9. The void area of unaligned images of Agisoft Metashape

The aerial triangulation results of four methods are shown in Figure 10. As can be seen from the Figure 10(*a*), after aerial triangulation, the proposed method shows that the main optical axis of the camera is basically vertical, the projection centers of all the images are basically in the same plane, and the aerial strips of photography are basically horizontal. These indicate that the shape of the horizontal ground and the surface of the PV panel has been basically restored correctly. The result of bundle adjustment based on the matched tie points is correct.

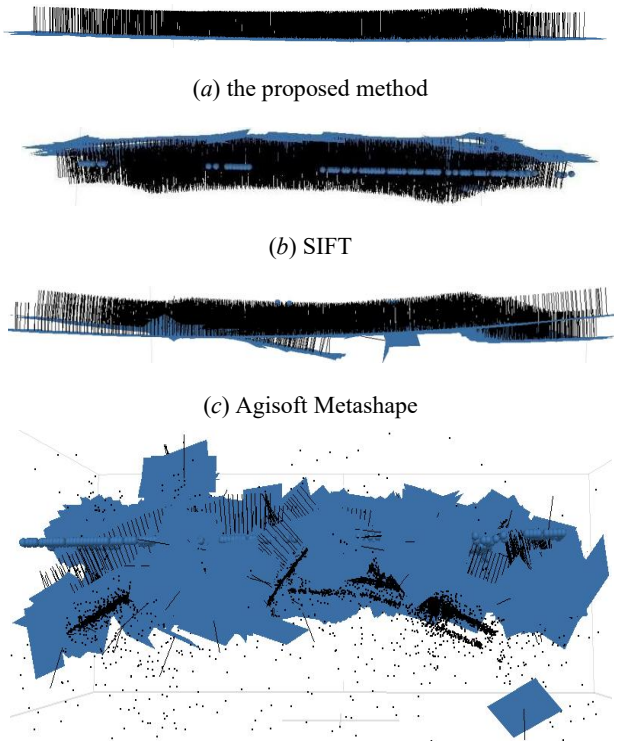

(*a*) the proposed method

(*b*) SIFT

(*c*) Agisoft Metashape

(*d*) COLMAP

Figure 10. The distributions of the adjusted camera positions of the proposed method and baseline methods

And in Figure 10(b), 10(c) and 10(d), some strips are not parallel to the ground, the main optical axes of some images are not vertical, and some images are not aligned. All of these phenomena indicate that there are more or less errors in the aerial triangulation results. So, the results are not reliable.

All in all, the proposed method not only significantly increases the number of extracted corresponding points, but also utilizes multiple methods and criteria, fully utilizing existing data. When removing gross errors, it fully considers the situation in three-dimensional space, greatly improving the horizontal accuracy and vertical accuracy in aerial triangulation results. This method not only avoids the occurrence of voids between images in the aerial triangulation results, but also perfectly integrates all images in the measurement area into the aerial triangulation network. The photography strip is also basically free of fluctuations, and the main optical axes of all images are almost entirely located in the vertical direction, as shown in Figure 9(a). Therefore, this is the most effective aerial triangulation result among the four methods.

4. Conclusion

This study proposed a sparse matching method based on the combination of point and line features to address the problem

of difficult matching of repetitive textures in thermal infrared images of PV panels. This method achieves matching between thermal infrared images of PV panels by extracting and matching line features, combined with geometric constraints of line features. The experimental results show that the proposed matching method outperformed SIFT, Agisoft Metashape, and COLMAP for thermal infrared images of PV panels on the number of total tie points, matching success rate and accuracy of matching reliability.

References

Romero-Cadaval E., Spagnuolo G., Franquelo L., Ramos-Paja C., 2013. Grid-Connected Photovoltaic Generation Plants: Components and Operation. *IEEE Industrial Electronics Magazine*. 7(3): 6-20.

Sun J.M., Liang L., Li G.D., Duan Z.Q., Hu W.S., 2022. Review of PV modules fault diagnosis technology. *Solar Energy*. (02): 12-22.

Hai T., Shangguan Y., Lu J., Wang J., Zhang T., 2023. Photovoltaic Panel Fault Detection Method Based on Optoelectronic Isolation and Frequency Detection. *Smart Power*. 51(08): 75-81+88.

Vergura S., Marino F., 2017. Quantitative and computer-aided thermography-based diagnostics for PV devices: part I - framework. *IEEE Journal of Photovoltaics*. 7(3): 822-827.

Jia S.K., 2021. Research on hot spot image detection method of photovoltaic modules based on residual attention mechanism. Baoding: North China Electric Power University.

Bu C.W., Liu T., Li R., Liu G.Z., Tang Q.J., 2022. Infrared Thermography Detection and Images Sequence Processing for Defection Photovoltaic Cells. *Acta Optica Sinica*. 42(7): 118-124.

Zhao Q., Liu S.J., Han D.C., Liu C.Y., Yang S.Z., 2023. Improved K-means Clustering-based Defect Detection Method for Photovoltaic Panels. *Infrared Technology*. 1-8.

Wang Y.Y., Li L.Y., Sun Y.F., Xu J.J., Jia Y., Hong J.Y., Hu X.B., Weng G.E., Luo X.J., Chen S.Q., Zhu Z.Q., Chu J.H., Akiyama H., 2021. Adaptive automatic solar cell defect detection and classification based on absolute electro-luminescence imaging. *Energy*. 229: 120606.

Liu G.S., Ding X., Zhu R., Zhang T.J., Di X.Y., Xue Z.H., 2023. Research on Extracting Photovoltaic Panels from High Resolution Remote Sensing Images by Combining HDC and Attention. *Computer Engineering and Applications*. 1-13.

Li B., Zhao K., Bai Y.S., Guo C.B., Chen N.H., Zhai Y.J., 2023. A Multi-scale Defect Detection Method for Photovoltaic Panels with Integrated Attention. *Electric Power Science and Engineering*. 39(08): 1-10.

Kaplani E., 2012. Detection of degradation effects in Field-aged c-Si solar cells through IR thermography and digital image processing. *International Journal of Photoenergy*. 396792.

Canny J.H., 1986. A computational approach to edge detection. *IEEE Transactions on Pattern Analysis and Machine Intelligence*. 8(6): 379-398.

Rafael G.V.G., Jeremie J., Jean-Michel M., Gregory R., 2010. LSD: a fast line segment detector with a false detection control. *IEEE Transactions on Pattern Analysis and Machine Intelligence*. 32(4): 722-32.

Zhang L.L., Koch R., 2013. An Efficient and Robust Line Segment Matching Approach Based on LBD Descriptor and Pairwise Geometric Consistency. *Journal of Visual Communication and Image Representation*. 24(7): 794-805.

Lowe D.G., 2004. Distinctive Image Features from Scale-Invariant Keypoints. *International Journal of Computer Vision*. 60(2): 91-110.

Bay H., Tuytelaars T., Gool L.V., 2006. SURF: speeded up robust features. Graz, Austria: *European Conference on Computer Vision*. 404-417.

Wu G.X., Yi C.L., Wu Z.G., 2024. Simulation of the Thermal Environment under Photovoltaic Panels with Spray Cooling. *Hydropower and New Energy*. 38(02): 25-28.

Du Y.P., Fell C.J., Duck B., Chen D., Liffman K., Zhang Y.N., Gu M., Zhu Y.G., 2016. Evaluation of photovoltaic panel temperature in realistic scenarios. *Energy Conversion and Management*. 108: 60-67.

Kurtz S., Whitfield K., Miller D., Joyce J., Zgonena T., 2009. Evaluation of high-temperature exposure of rack-mounted photovoltaic modules. *Proceedings of the 2009 34th IEEE Photovoltaic Specialists Conference (PVSC)*. F7-12.

Zhang J.Q., Pan L., Wang S.G., 2009. *Photogrammetry (Edition 2)*.

Schonberger J. L., Frahm J. M., 2016. Structure-from-motion revisited. In *Proceedings of the IEEE Conference on Computer Vision and Pattern Recognition*. 4104-4113.